

# Battle of the Predictive Wavefront Controls: Comparing Data and Model-Driven Predictive Control for High Contrast Imaging



Fowler<sup>1</sup>, J., van Kooten<sup>1</sup>, M.A.M., Jensen-Clem<sup>1</sup>, R.  
University of California, Santa Cruz<sup>1</sup>



## Preliminary Result: On-Sky Telemetry

We find an improvement of  $\sim 1.2$  from using predictive Fourier control (the model-driven method) when applied to on-sky telemetry from Keck.

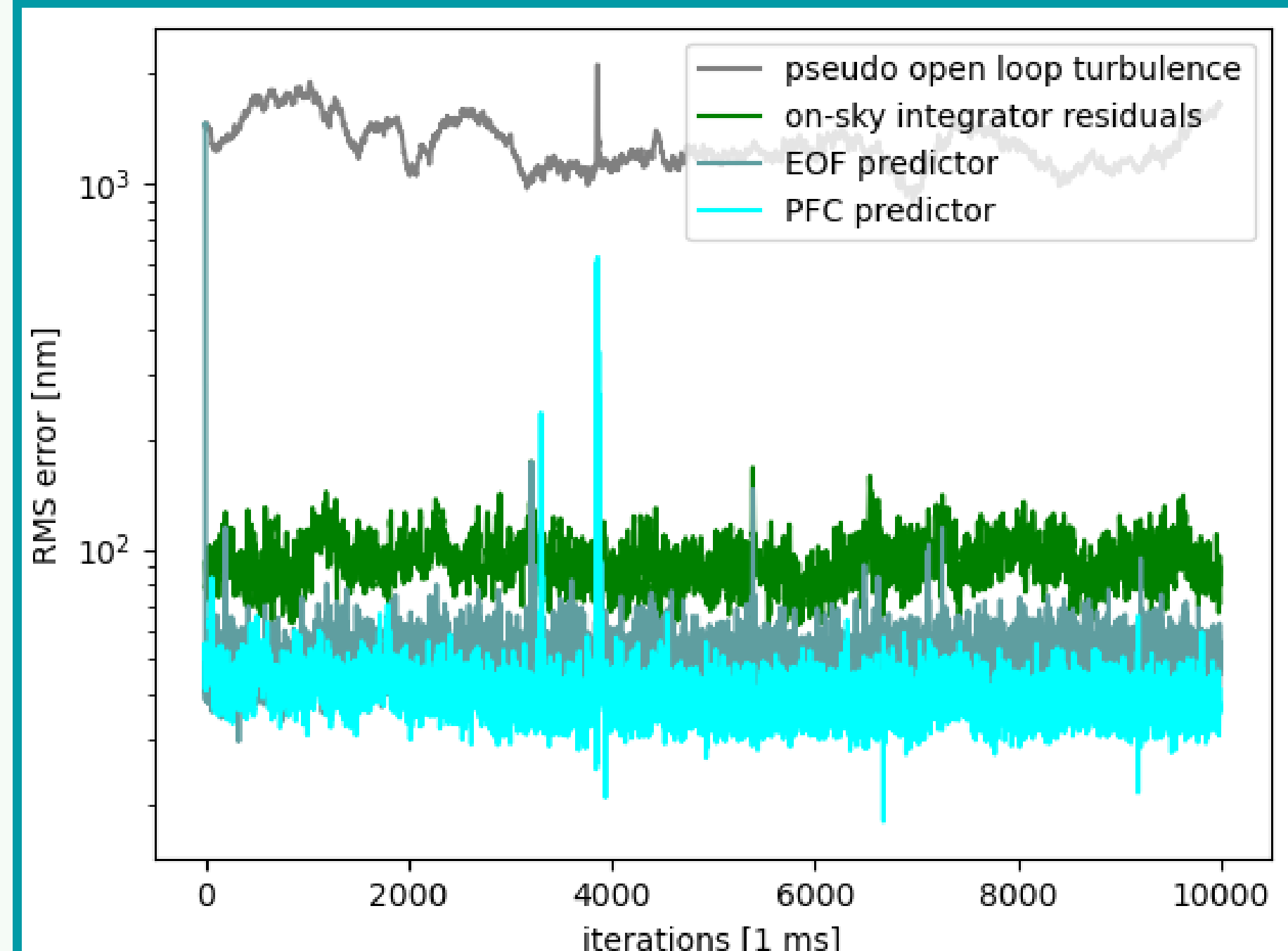


Figure 1: Uncorrected turbulence:  $1243 \pm 192$  nm, integrator:  $91.21 \pm 12.97$  nm, EOF predictor:  $48.99 \pm 15.33$  nm, PFC predictor:  $39.07 \pm 15.33$  nm.

## Predictive Fourier Control

Predictive Fourier control (Poyneer, 2007) starts with decomposing turbulence into complex Fourier modes, for some mode indexed  $(k, l)$ , over a grid of  $m$  by  $n$  pixels:

$$f_{k,l}[m, n] = \cos\left(2\pi \frac{kx + ly}{N}\right) + i\sin\left(2\pi \frac{kx + ly}{N}\right) \quad (1)$$

for  $N$  total modes. Each Fourier mode becomes its own control problem, for which we:

- ➊ create a power spectral density (PSD) function by taking a Fourier transform in temporal frequency space
- ➋ fit each peak in the PSD with complex coefficients
- ➌ feed those complex coefficients to a predictive Kalman filter, modified to run an open-loop control law

### (1) Wind Layer Identification

We identify wind layers in the atmosphere as pupil crossing frequencies in the power spectral density (PSD) function. Frequencies at some  $(k, l)$  mode map to wind layers moving at  $(v_x, v_y)$ :

$$\nu = -\left(\frac{kv_x + lv_y}{D}\right) \quad (2)$$

where  $D$  is the telescope primary diameter.

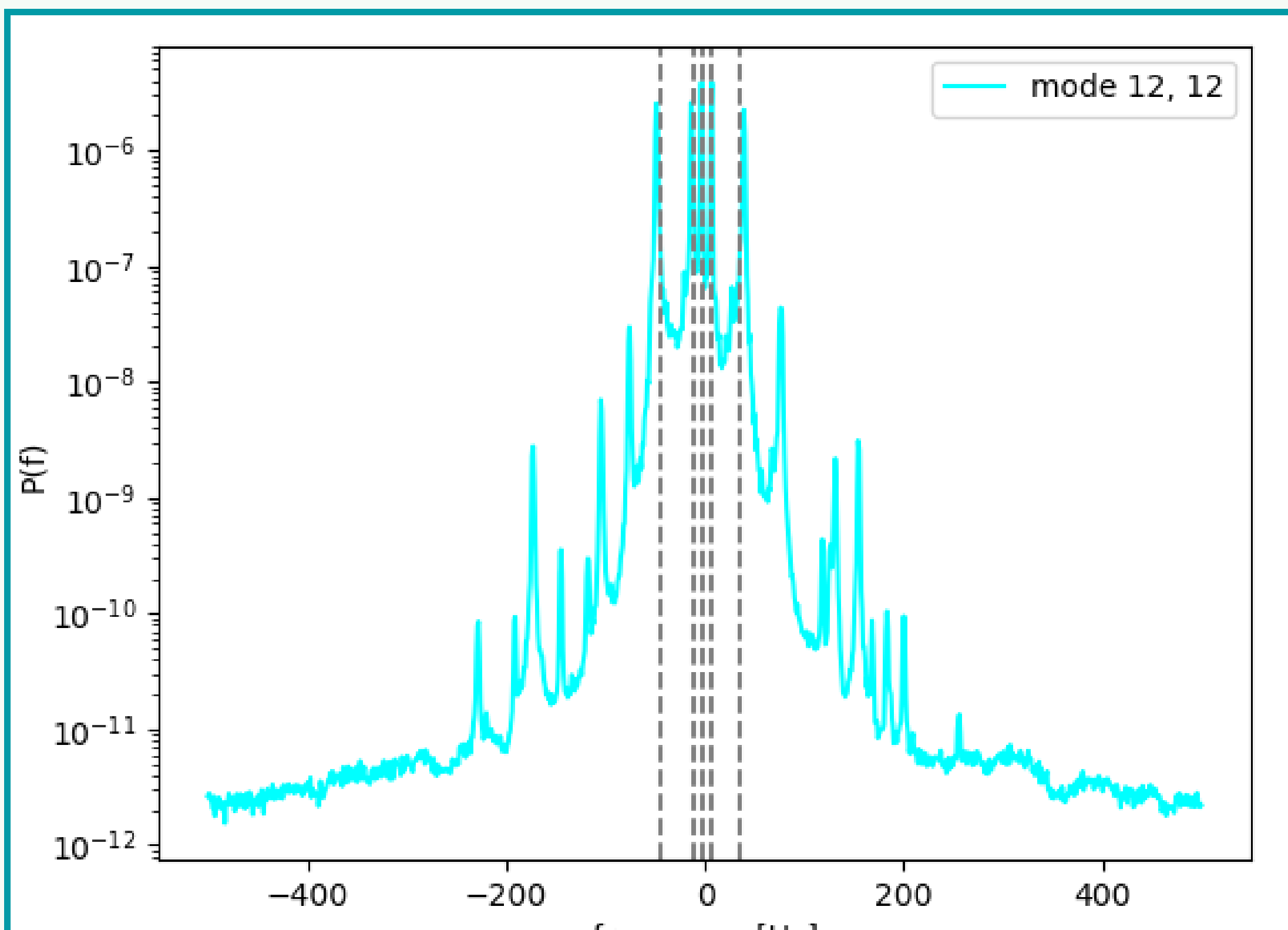


Figure 2: Here we correctly identify all 5 wind layers from our simulated atmosphere for the (12,12) mode. The dashed lines indicate injected wind layers, which align with peaks in the PSD.

### (2) Peak Fitting

We fit each peak with:

$$P(\omega) = \frac{\sigma^2}{|1 - \alpha e^{(-i\omega)t}|^2} \quad (3)$$

given complex  $\alpha = |\alpha|e^{i\phi}$ .  $\alpha$  and  $\sigma$  describe the placement (i.e., velocity) and strength of the wind layers, respectively.

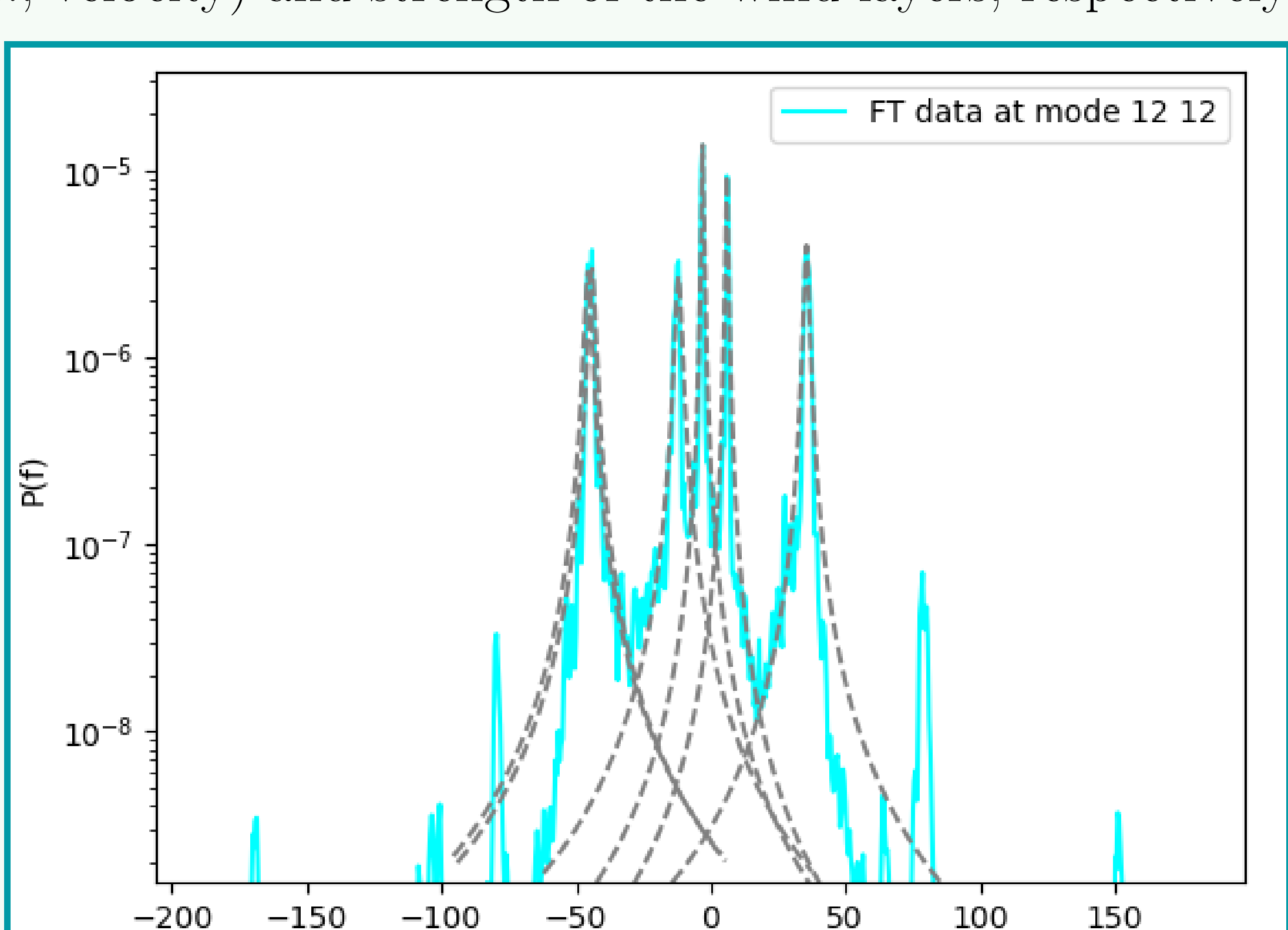


Figure 3: From the same data as Figure 2. The dashed lines represent the functional form of each peak fit with  $\alpha$  and  $\sigma$ , as it corresponds to the PSD.

## Abstract

Ground-based high contrast exoplanet imaging requires state-of-the-art adaptive optics (AO) systems in order to detect extremely faint planets next to their brighter host stars. For extreme AO systems (with high actuator count deformable mirrors), wavefront errors at small angular separations from the host star are often dominated by the lag time of the correction (i.e., the amount the wavefront has changed by the time the system is able to apply the correction) which can be anywhere from 1-5 milliseconds. One solution is predictive control, wherein previous wavefront information is used to predict the future state of the wavefront in one-system-lag's time, and this predicted state is applied as a correction. Here, we consider two methods for predictive control: data-driven prediction using empirical orthogonal functions (EOF) and the physically-motivated predictive Fourier control. The performance and robustness of these methods have not previously been compared side-by-side. We compare these methods in simulation, to better understand the circumstances in which their performance differs, including testing them under different wind speeds and atmospheric profiles. For extremely large telescopes like the European Extremely Large Telescope and the Thirty Meter Telescope, predictive control is included as a key element to reach the contrast needed to image a rocky earth-like planet.

## Wind-Driven Halos Impact Coronagraphic Images

The 1-4 ms time lag in an adaptive optics control loop is plenty of time for layers of wind to blow a correction into history.

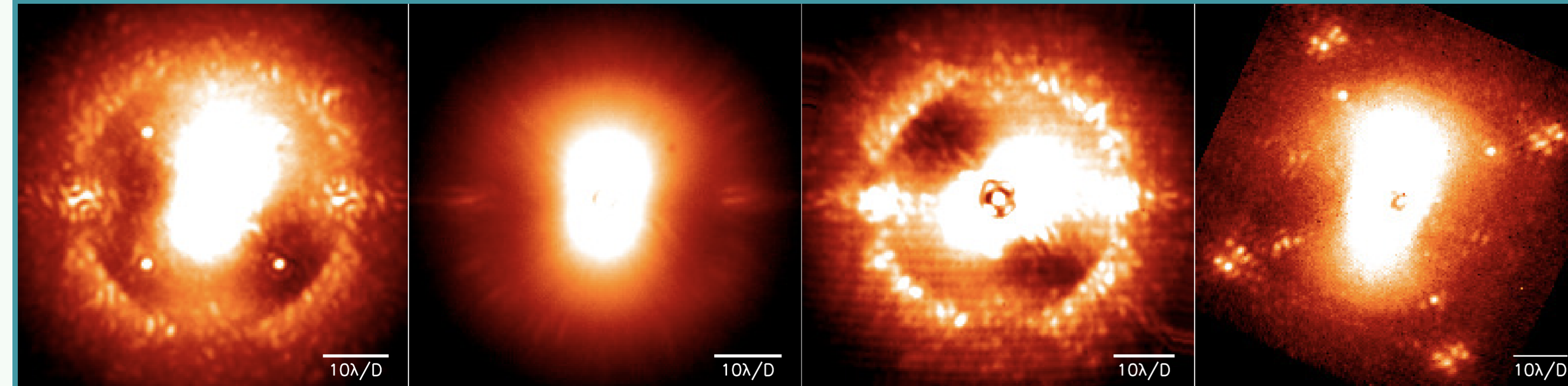


Figure 4: Figure from Cantalloube, 2018, showing wind-driven halos in SPHERE (left-most 3) and GPI (right-most) coronagraphic images. These asymmetric halos are difficult to remove with post-processing and obscure the dark-hole within  $10\lambda_D$ .

## Time Lag in Adaptive Optics Systems

The length of the wavefront sensor exposure (1), the calculation time of the computer (2), and the response time of the deformable mirror (3) all make up a system time lag, i.e., for Keck Observatory this is 1.7 ms (Cetre, 2018).

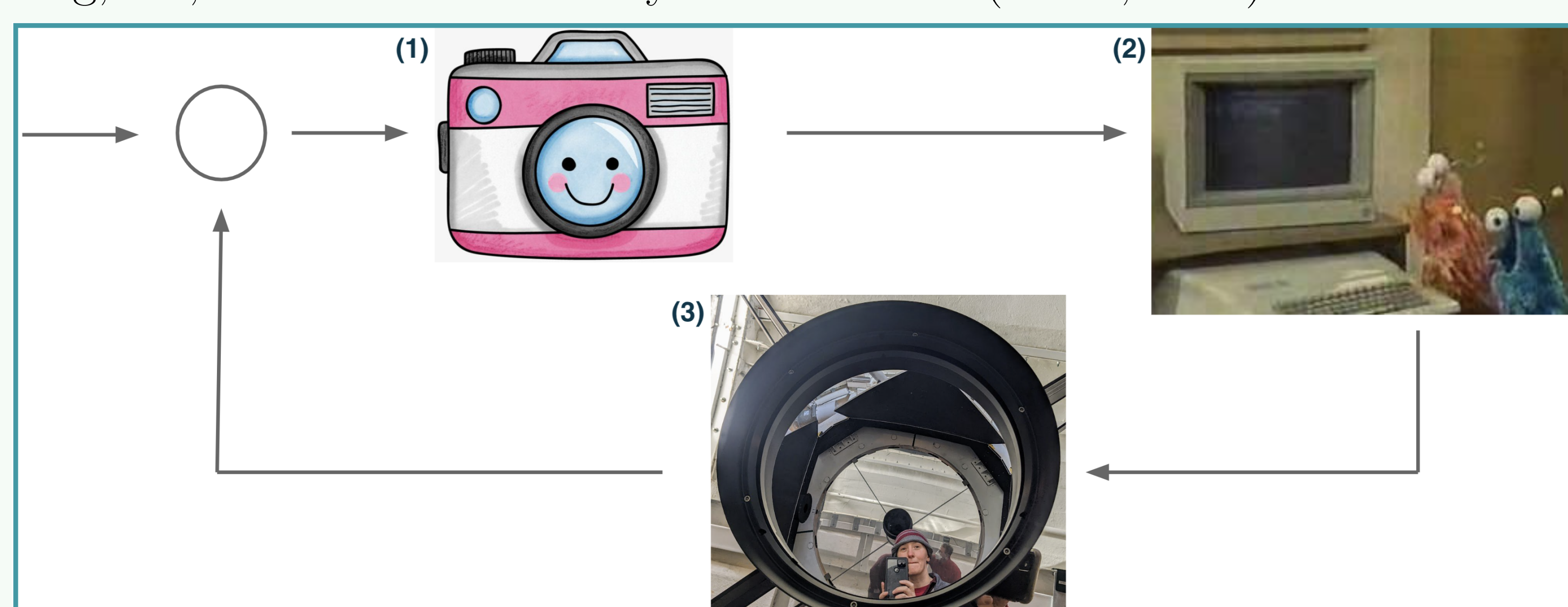


Figure 5: Cartoon AO control loop with a (1) wavefront sensor, (2) computer, and (3) deformable mirror.

## (3) Predictive Kalman Filtering

We use a Kalman Filter to predict the state vector  $\mathbf{x}$ :

$$\mathbf{x}[t] = (\mathbf{a}[t], \phi[t+1], \phi[t], \phi[t-1], d[t-1], d[t-2])^T \quad (4)$$

where  $\phi$  is the wavefront at some time,  $d$  is the command to the deformable mirror, and  $\mathbf{a}$  is a vector encapsulating each wind layer for a given mode.

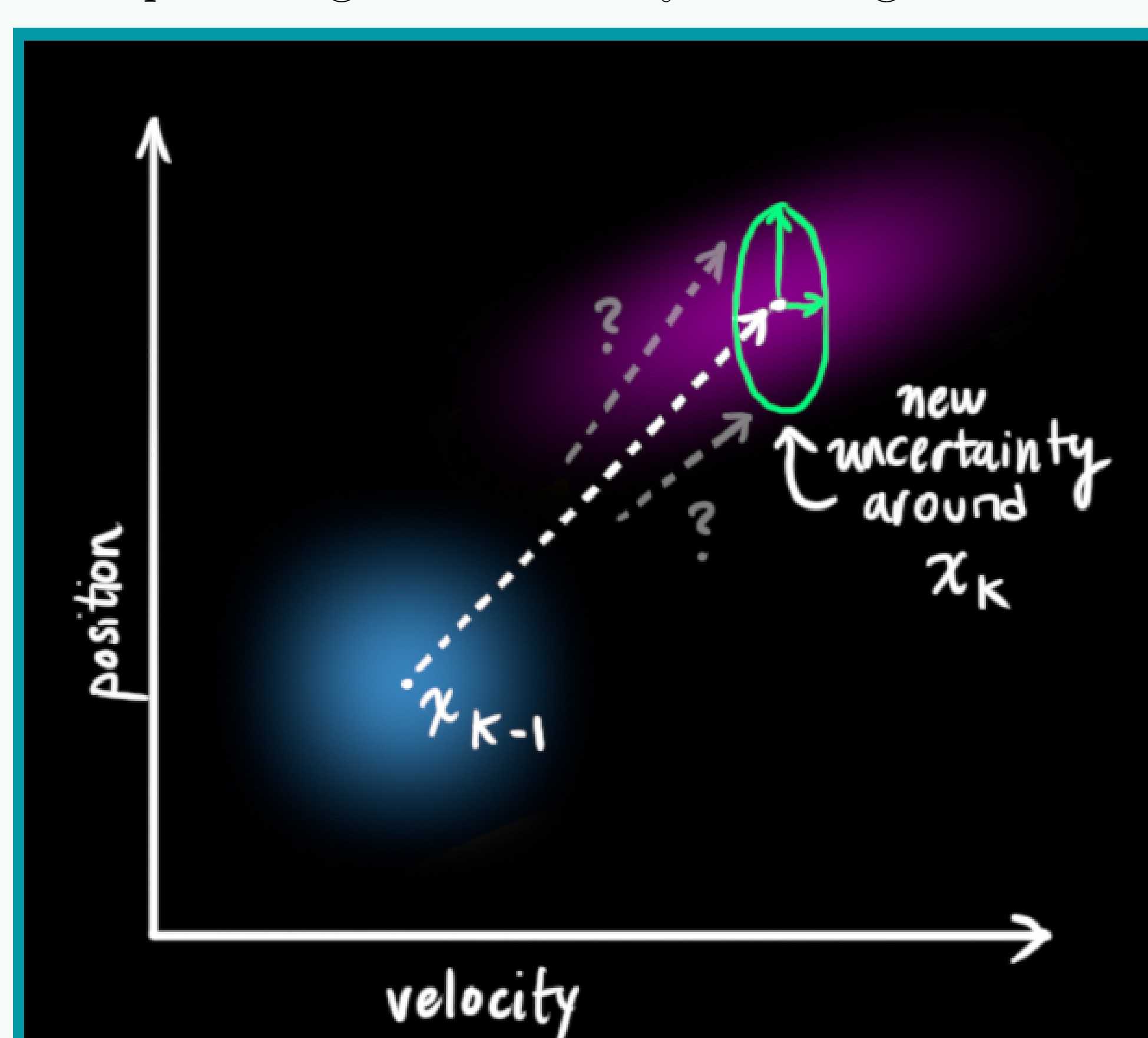


Figure 6: Figure from Tim Babb's bzarg, demonstrating a generalized Kalman filter predicting both a system state and its covariance.

## Preliminary Result: Simulated Single-Layer Atmosphere

We find an improvement of  $\sim 4$  from empirical orthogonal functions (the data-driven method) when applied to a simulated atmosphere with a single 7 m/s wind layer.

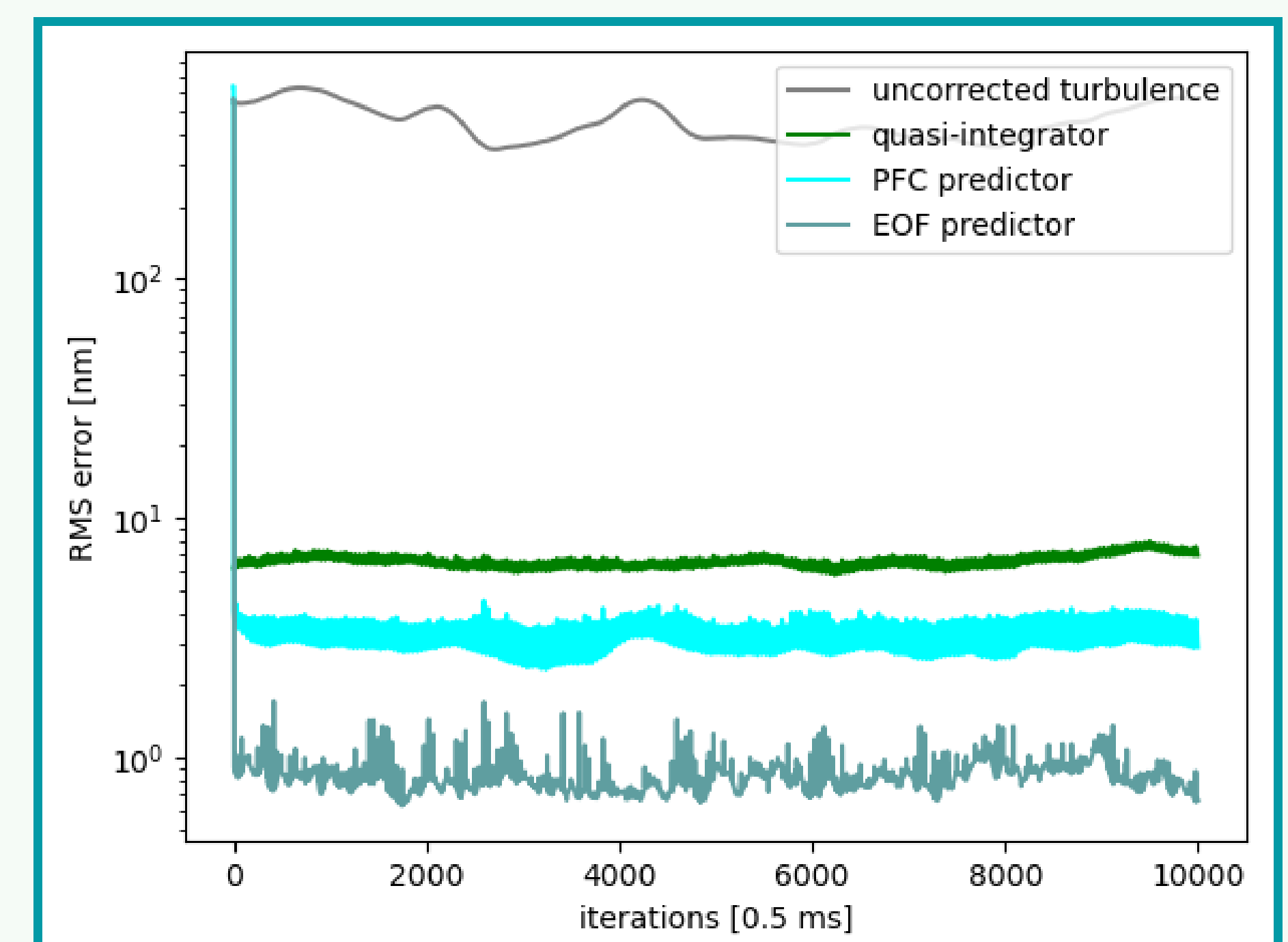


Figure 7: Uncorrected turbulence:  $429.74 \pm 79$  nm, integrator:  $6.58 \pm 0.4$  nm, PFC predictor:  $3.30 \pm 0.4$  nm, EOF predictor:  $0.80 \pm 0.1$  nm.

## Empirical Orthogonal Functions

Empirical orthogonal functions (Guyon, 2017) breaks down wavefront prediction as a single linear algebra problem.  $\mathbf{D}$  and  $\mathbf{P}$  contain history vectors  $\mathbf{h}$  with previous states of the wavefront and the future state of the wavefront, respectively. We use a least squares inversion to find the predictive filter  $\mathbf{F}$  with regularization constant  $\alpha$ .

$$\min ||\mathbf{D}^T \mathbf{F}^T - \mathbf{P}^T||^2 \quad (5)$$

$$\mathbf{F} = ((\mathbf{D}^T)^{\dagger} \mathbf{P}^T)^T \quad (6)$$

$$\mathbf{F} = \mathbf{P} \mathbf{D}^T (\mathbf{D} \mathbf{D}^T + \alpha \mathbf{I})^{-1} \quad (7)$$

$$\text{prediction} = \mathbf{F} \mathbf{h} \quad (8)$$

## Uncorrected, Integrator, and Predictor Performance

A visual example of residual error from Keck telemetry over a telescope pupil when corrected by a typical integrator vs. an EOF-style predictor.

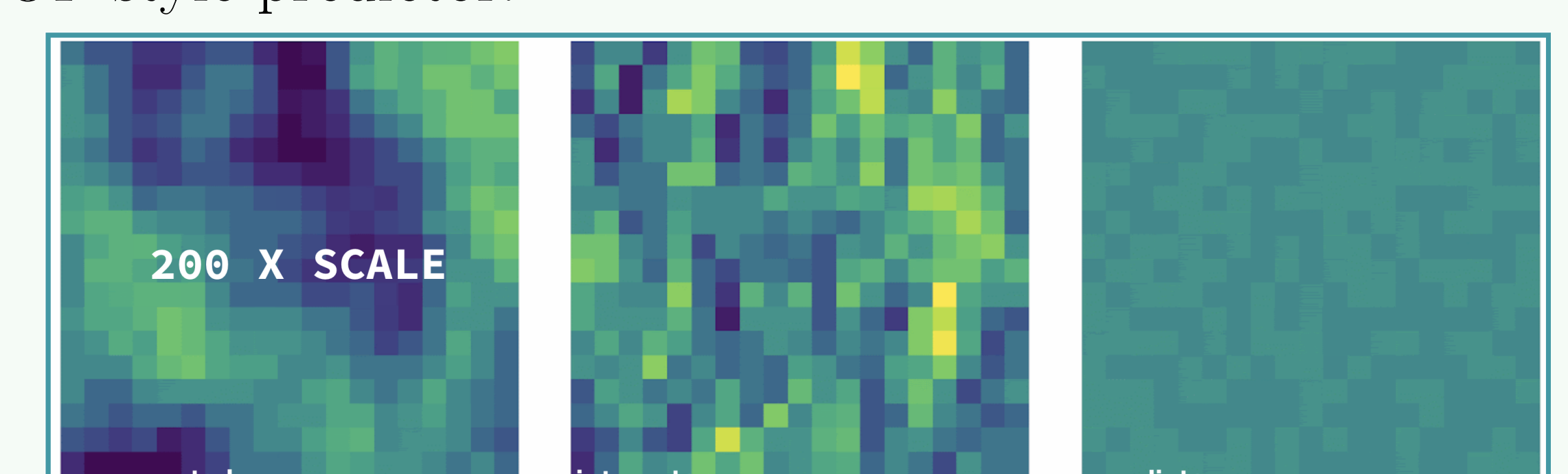


Figure 8: Left: Phase from uncorrected open-loop turbulence from Keck. (Note 200x scale as compared to right two images.) Middle: Typical integrator control residuals. Right: EOF prediction residuals. For ease of plotting, we've taken square cutouts over circular telescope pupils.

## Conclusions and Future Work

Our preliminary results find that empirical orthogonal functions performs better than predictive Fourier control for simple atmospheric models, but predictive Fourier control has a subtle advantage when applied to on-sky telemetry. Next steps include:

- further optimization of predictive Fourier control
- computational benchmarking
- testing these methods on a high-fidelity Keck-AO simulation
- testing these methods on the Santa Cruz Extreme AO Laboratory (SEAL) testbed

## Contact Information

- twitter: @121gigajules
- email: jumfowle@ucsc.edu

## References

- Bzarg, How a Kalman filter works, in pictures
- Cantalloube, 2021, Origin of the asymmetry of the wind driven halo observed in high contrast images
- Cetre, 2018, A near-infrared pyramid wavefront sensor for Keck adaptive optics: real-time controller
- Guyon, 2017, Adaptive Optics Predictive Control with Empirical Orthogonal Functions (EOFs)
- Poyneer, 2007, Fourier transform wavefront control with adaptive prediction of the atmosphere